Bioactive Materials 6 (2021) 3097–3108

Contents lists available at ScienceDirect

Bioactive Materials

journal homepage: www.sciencedirect.com/journal/bioactive-materials

Effect of cyclic mechanical loading on immunoinflammatory microenvironment in biofabricating hydroxyapatite scaffold for bone regeneration

Penghui Zhang [a,b,1], Xizhe Liu [b,1], Peng Guo [a,b,1], Xianlong Li [a,b], Zhongyuan He [a,b], Zhen Li [c], Martin J. Stoddart [c], Sibylle Grad [c], Wei Tian [d], Dafu Chen [d,***], Xuenong Zou [b,**], Zhiyu Zhou [a,b,*], Shaoyu Liu [a,b]

[a] Innovation Platform of Regeneration and Repair of Spinal Cord and Nerve Injury, Department of Orthopaedic Surgery, The Seventh Affiliated Hospital, Sun Yat-sen University, Shenzhen, 518107, China
[b] Guangdong Provincial Key Laboratory of Orthopedics and Traumatology, Orthopaedic Research Institute /Department of Spinal Surgery, The First Affiliated Hospital of Sun Yat-sen University, Guangzhou, 510080, China
[c] AO Research Institute Davos, Clavadelerstrasse 8, Davos, 7270, Switzerland
[d] Laboratory of Bone Tissue Engineering, Beijing Laboratory of Biomedical Materials, Beijing Research Institute of Orthopaedics and Traumatology, Beijing JiShuiTan Hospital, Beijing, 100035, China

ARTICLE INFO

Keywords:
Bioreactor
Biofabrication
Inflammatory microenvironment
Bone biomaterials
Macrophage polarization

ABSTRACT

It has been proven that the mechanical microenvironment can impact the differentiation of mesenchymal stem cells (MSCs). However, the effect of mechanical stimuli in biofabricating hydroxyapatite scaffolds on the inflammatory response of MSCs remains unclear. This study aimed to investigate the effect of mechanical loading on the inflammatory response of MSCs seeded on scaffolds. Cyclic mechanical loading was applied to biofabricate the cell-scaffold composite for 15 min/day over 7, 14, or 21 days. At the predetermined time points, culture supernatant was collected for inflammatory mediator detection, and gene expression was analyzed by qRT-PCR. The results showed that the expression of inflammatory mediators (*IL1B* and IL8) was downregulated ($p < 0.05$) and the expression of *ALP* ($p < 0.01$) and *COL1A1* ($p < 0.05$) was upregulated under mechanical loading. The cell-scaffold composites biofabricated with or without mechanical loading were freeze-dried to prepare extracellular matrix-based scaffolds (ECM-based scaffolds). Murine macrophages were seeded on the ECM-based scaffolds to evaluate their polarization. The ECM-based scaffolds that were biofabricated with mechanical loading before freeze-drying enhanced the expression of M2 polarization-related biomarkers (*Arginase 1* and *Mrc1*, $p < 0.05$) of macrophages in vitro and increased bone volume/total volume ratio in vivo. Overall, these findings demonstrated that mechanical loading could dually modulate the inflammatory responses and osteogenic differentiation of MSCs. Besides, the ECM-based scaffolds that were biofabricated with mechanical loading before freeze-drying facilitated the M2 polarization of macrophages in vitro and bone regeneration in vivo. Mechanical loading may be a promising biofabrication strategy for bone biomaterials.

Peer review under responsibility of KeAi Communications Co., Ltd.
* Corresponding author. Innovation Platform of Regeneration and Repair of Spinal Cord and Nerve Injury, Department of Orthopaedic Surgery, The Seventh Affiliated Hospital, Sun Yat-sen University, 518107, Shenzhen, China.
** Corresponding author.
*** Corresponding author.
E-mail addresses: zhangph7@mail2.sysu.edu.cn (P. Zhang), gzxzhliu@qq.com (X. Liu), guopeng@mail2.sysu.edu.cn (P. Guo), lixlong33@mail2.sysu.edu.cn (X. Li), hezhy37@mail2.sysu.edu.cn (Z. He), zhen.li@aofoundation.org (Z. Li), martin.stoddart@aofoundation.org (M.J. Stoddart), sibylle.grad@aofoundation.org (S. Grad), tianweijst@vip.163.com (W. Tian), chendafujst@126.com (D. Chen), zxnong@hotmail.com, zouxuen@mail.sysu.edu.cn (X. Zou), zhouzhy23@mail.sysu.edu.cn (Z. Zhou), gzsyliu@tom.com (S. Liu).
[1] These authors contributed equally to this work.

https://doi.org/10.1016/j.bioactmat.2021.02.024
Received 4 November 2020; Received in revised form 18 February 2021; Accepted 18 February 2021
Available online 9 March 2021

1. Introduction

With a global trend of population aging, there has been significant growth in the clinical demand for bone grafts as a result of the steep increase in the incidences of bone trauma and bone diseases [1,2]. Although current strategies using autologous or allogeneic bone grafts are the most common choice for bone defect repair, they have failed to fulfill the clinical demand. Limited availability and donor-site morbidity remain unsolved problems related to the use of autografts [3,4], and the potential risk of disease transmission, infection, and immune rejection restricts the application of allografts [5]. Bone tissue engineering aims to overcome the drawbacks of traditional bone regeneration techniques and has been considered a promising approach for the development of tissue-engineered bone grafts.

Previous studies have focused on improving the biocompatibility and osteogenic effect of bone biomaterials by modifying physical or chemical properties. Tuning the topology of biomaterials could improve their biocompatibility and ameliorate the induced immune-mediated reaction to enhance bone regeneration [6–8]. Biomaterials loaded with bioactive agents can achieve dual anti-inflammatory and osteogenic effects [9,10]. Additionally, biomimetic hydroxyapatite-based composites can significantly enhance bone regeneration without inducing obvious inflammatory responses in vivo [11,12]. However, bone biomaterials with excellent performance require an osteoconductive scaffold composed of extracellular matrix (ECM) to simulate the natural environment [13], since ECM sustains a precise and ordered network structure and provides a microenvironment that supports the growth and differentiation of cells in vivo [14]. Obviously, compared with the modification of a single physical or chemical property of a biomaterial, more comprehensive manipulation of the surface structure and bioactive component of biomaterials could be achieved via in vitro cell-derived ECM biofabrication [15]. Thus, ECM-based biomaterials are considered to be promising for use in tissue engineering [16–19].

Previously, our group constructed a biofabricated hydroxyapatite scaffold that was modified with extracellular matrix contained LIM mineralization protein-1 under static culture conditions, and in vivo and in vitro studies showed that the scaffold has a favorable osteogenic effect [20]. Theoretically, the ECM content after 14 or 21 days of cell-scaffold culture should be greater than that after 7 days, which would be more beneficial for osteogenesis. Contrary to expectations, osteogenesis in vivo was reduced after the implantation of 14- and 21- day modified ECM-based scaffolds as a result of the excessive inflammatory response. These results suggested that the conventional strategies of bone tissue engineering, which depended solely on biochemical cues to instruct biomaterial development, were in need of improvement.

The mechanical microenvironment is an indispensable factor for the regeneration and remodeling of bone tissue. Wolff's law states that bone tissue adapts to the mechanical loading under which it is placed. It has become a consensus that appropriate mechanical stimuli can promote osteogenesis. Notably, compressive force represents the predominant mechanical stimulus acting on bone cells in vivo [21], although bone tissue experiences a variety of mechanical forces, including pressure, strain, shear, and torsion [22]. It has been shown that the compressive mechanical loading of 3D cellular scaffolds can improve cellular proliferation, osteogenic differentiation and even neovascularization [23–26]. Furthermore, mechanical stimuli delivered by bioreactors to develop tissue constructs can influence the adaptation of the construct itself to the physiological mechanical microenvironment after implantation [27,28]. Therefore, bioreactor systems can be used to apply mechanical stimuli to 3D tissue constructs to study the role of the mechanical microenvironment on cellular fate in vitro and improve the performance of engineered biomaterials in vivo [25,29,30].

It is well known that the immunoinflammatory microenvironment induced by bone grafts is one of the critical factors affecting bone repair. Unexpected inflammation (as demonstrated in our previous study [20]) and foreign body reactions restrict the clinical application of bone grafts [31,32]. Recently, it was reported that PIEZO1, an important mechanical signal-related protein, was involved in promoting the secretion of a variety of bioactive factors and regulating immune cell function under conditions of mechanical stimulation [33]. Albarran-Juarez et al. [34] found that different mechanical loading protocols had different regulatory effects on the inflammatory response. However, the immunoinflammatory property of bone biomaterials determined by the effect of mechanical stimuli is not yet fully understood.

Therefore, to study the effect of mechanical loading in biofabricating bone biomaterials on the inflammatory-modulation and osteogenesis of MSCs seeded on 3D scaffolds, we hypothesized that the application of mechanical loading in biofabricating cell-scaffold composites would be beneficial in terms of the immunoinflammatory properties. In this study, human umbilical cord mesenchymal stem cells (hUCMSCs) were seeded on 3D natural porous hydroxyapatite scaffolds, and mechanical stimuli were applied to the cell-scaffold composites in a compressive mechanical loading bioreactor system for 15 min/day over 7, 14 or 21 days; then, the effect on various parameters of inflammation and osteogenic differentiation was analyzed. Static groups comprised scaffolds biofabricated under the same conditions without mechanical loading, which were used as controls. Meanwhile, the cell-scaffold composites biofabricated with or without mechanical loading were freeze-dried to prepare ECM-based scaffolds. A murine macrophage in vitro model was further used to evaluate the anti-inflammatory and regenerative effects of these ECM-based scaffolds. A rabbit femoral condyle bone defect model was established to assess the efficacy of these ECM-based scaffolds in bone defect repair after 1 and 8 weeks of implantation.

2. Materials and methods

2.1. hUCMSC isolation, expansion, and characterization

The experimental protocols used in this study were reviewed and approved by the Ethics Committee of the Seventh Affiliated Hospital of Sun Yat-sen University (Permit Number: 2019SYSUSH-031) and written informed consent was obtained from all healthy women. Based on a previous study with minor modifications [35], MSCs were isolated from the Wharton's jelly of human umbilical cords and cells at passages 3 to 5 were used for this study. Briefly, umbilical cords were collected within 4 h after delivery and rinsed three times with phosphate-buffered saline (PBS) containing 2% v/v penicillin/streptomycin. Umbilical cord blood vessels were removed from the Wharton's jelly. Then the Wharton's jelly was minced into pieces approximately 1 mm^3 in size and cultured in serum-free medium for MSCs (Prim® hMSC SF-M, Premedical Laboratories Co., Ltd., Beijing, China) at 37 °C in a 5% CO2 humidified incubator. The medium was replaced every 3 days, and the cells were subcultured when approximately 80% confluent.

For characterization of the cellular immunophenotype, cell surface staining was performed with phycoerythrin-conjugated antibodies against CD19 and CD105, allophycocyanin-conjugated antibodies against CD34, CD45, and CD90, or fluorescein isothiocyanate-conjugated antibodies against CD73 and human leukocyte antigen (HLA)-DR (all products from BioLegend, San Diego, CA, USA). Fluorescence was measured by flow cytometry (CytoFLEX LX, Beckman Coulter, Indianapolis, USA), and the data were analyzed using CytExpert 2.3 software (Beckman Coulter, USA).

For osteogenic and adipogenic differentiation, cells were cultured for 21 days in MSC osteogenic medium (MSC osteogenesis kit, BGsciences, Guangzhou, China) and adipogenic medium (MSC adipogenesis kit, BGsciences, Guangzhou, China). Differentiation medium was used in accordance with the manufacturer's protocols. Alizarin red (from the MSC osteogenesis kit) staining and oil red O (from the MSC adipogenesis kit) staining were performed to verify the osteogenic and adipogenic differentiation of MSCs, respectively.

2.2. Preparation of hydroxyapatite scaffolds

Natural hydroxyapatite scaffolds were prepared by calcining the cancellous bone of bovine vertebra (Fig. 3A–B), as previously described [20]. Scaffolds were cut into a cylindrical shape with 4.5 mm in diameter and 10 mm in height (Fig. 1 A) and sterilized with ethylene oxide before use.

2.3. Cell seeding and culturing on scaffolds

hUCMSCs were seeded on the scaffolds according to our previously described methods with minor modifications [20]. Briefly, sterilized scaffolds were covered completely in the cell suspension at a density of 1×10^7 cells/mL and were then treated with low-pressure conditions utilizing a vacuum freeze dryer (SCIENTZ-10ND, China). After 4 h of incubation at 37 °C in a 5% CO2 humidified incubator, the cell-scaffold composites were transferred into 24-well plates and cultured in serum-free medium for human MSCs (Prim® hMSC SF-M, Premedical Laboratories Co., Ltd., Beijing, China). After 48 h of culture, the medium was changed to osteogenic-induction medium supplemented with 100 nM dexamethasone, 10 mM β-glycerophosphate, and 50 μg/mL ascorbic acid 2-phosphate (all products from Sigma-Aldrich, St Louis, MO, USA). Subsequently, the cell-scaffold composites were cultured under static or cyclic mechanical loading conditions, and the medium was replenished once a day.

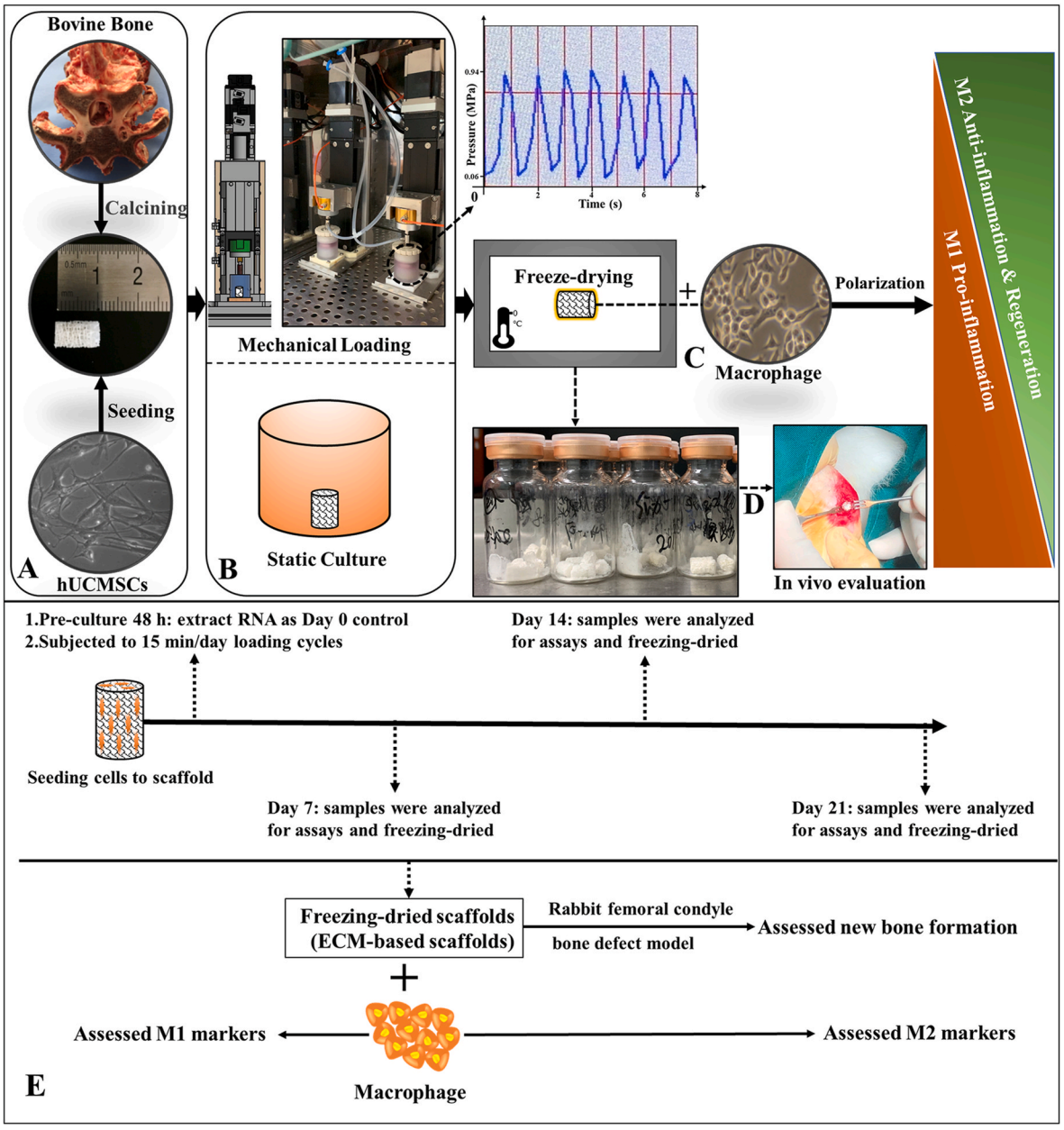

Fig. 1. Scheme of experimental setup. **A)** The cancellous bone of bovine vertebra was sintered and cut into a cylindrical shape; hUCMSCs were seeded on natural 3D scaffold. **B)** Cell-scaffold composites were cultured in a compressive loading bioreactor (0.06–0.94 MPa; 1 Hz; 15 min/day), and static culture was acted as control. **C)** Cell-scaffold composites were freeze-dried to obtain ECM-based scaffolds, and the effect of ECM-based scaffolds on macrophage polarization was assessed. **D)** A rabbit femoral condyle bone defect model was established to assess the efficacy of these ECM-based scaffolds in bone defect repair. **E)** Experimental design for harvesting samples and assays.

2.4. Cyclic mechanical loading of cell-scaffold composite

Cyclic mechanical loading of the cell-scaffold composites was applied through a custom-designed bioreactor system (manufactured), similarly described by Gantenbein et al. [36] and Illien-Junger et al. [37]. The cell-scaffold composites in the bioreactor chamber were biofabricated with a linear wave of cyclic mechanical compression (Fig. 1 B) at a frequency of 1 Hz and a magnitude of 0.06 MPa–0.94 MPa for 15 min/day over 7, 14, or 21 days; the loading parameters were set partly in reference to the previous studies [38,39] and the results of our preliminary experiments. The cell-scaffold composites were harvested on day 7, 14, or 21 and denoted as the Loading-7d, Loading-14d, or Loading-21d group, respectively. Static groups comprised scaffolds treated under the same conditions without mechanical loading over 7, 14 or 21 days, which were denoted as the Static-7d, Static-14d, and Static-21d group, respectively.

2.5. Cell viability and proliferation

All cell-scaffold composites were preliminarily evaluated under a stereomicroscope (OLYMPUS SZX10, Japan). Cell viability was assessed by calculating the live cell ratio. In brief, cell-scaffold composites were rinsed with PBS and stained with Hoechst 33342 (Invitrogen, Carlsbad, CA, USA) and a Calcein-AM/PI double staining kit (US EVERBRIGHT, Suzhou, China). Images were captured using a fluorescence microscope (Leica DMi8, Germany). PI- and Hoechst-positive cells in the entire field of 3 randomly selected views were counted, and the live cell ratio was calculated. Specifically, the live cell ratio equaled one minus (PI-positive cells/Hoechst-positive cells). The total DNA content was determined to obtain indirect information about cellular proliferation. The cellular DNA content was measured using a PicoGreen dsDNA quantification kit (LIFE iL AB BIO, Shanghai, China) according to the instructions of the manufacturer. DNA was extracted by proteinase K solution (APExBio, Houston, USA) at a concentration of 1 mg/mL at 56 °C overnight. The extracted DNA solution was incubated in PicoGreen dsDNA working solution at room temperature in the dark for 10 min, after which the fluorescence excitation/emission at 350/460 nm was read by microplate reader (BioTek Synergy H1, USA).

2.6. Proteome Profiler Array evaluation of inflammatory mediator expression

Cell culture supernatants were harvested on days 7, 14 and 21. Human array kits for inflammatory markers (R&D Systems ARY0017, USA) were used following the manufacturer's protocols. In brief, microarray films were blocked with blocking buffer at room temperature for 30 min and incubated for 1 h on a shaker. The samples were mixed with a cocktail of biotinylated detection antibodies and incubated overnight with membranes at 4 °C. After the membranes were washed three times, streptavidin-HRP was added and incubated with membranes for 30 min at room temperature on a shaker. After another wash, chemiluminescent detection reagents were used, images were captured, and signal strength data were analyzed with a ChemiDocXRS + system (Bio-Rad, USA). The pixel density produced at each capture spot corresponded to the amount of target protein bound. Relative values of target protein expression were obtained by normalization to the DNA quantification data. A Proteome Profiler Array was applied once to preliminarily screen out the highly expressed proinflammatory proteins. The five proteins with the highest expression were further analyzed by quantitative real-time polymerase chain reaction (qRT-PCR).

2.7. Preparation of ECM-based scaffolds by freeze-drying of cell-scaffold composites

The cell-scaffold composites that were biofabricated with mechanical loading or static culture for 7 days, 14 days, or 21 days were freeze-dried using a freeze-dryer (SCIENTZ-10ND, China) to prepare ECM-based scaffolds retaining the bioactive factors of ECM according to our previous protocol [20]. Meanwhile, the groups of ECM-based scaffolds that were prepared from the cell-scaffold composites in the Loading-7d, Loading-14d, and Loading-21d groups were denoted as E-Loading-7d, E-Loading-14d, and E-Loading-21d, respectively. The groups of ECM-based scaffolds that were prepared from the cell-scaffold composites in the Static-7d, Static-14d, and Static-21d groups were denoted as E-Static-7d, E-Static-14d, and E-Static-21d, respectively. The ECM-based scaffolds were stored in −80 °C freezer until further use.

2.8. Polarization of macrophage seeded on the ECM-based scaffolds

RAW 264.7 murine macrophage (FuHeng, Shanghai, China) were used in the present study and cultured in high-glucose Dulbecco's modified Eagle medium (Gibco, Suzhou, China) supplemented with 5% fetal bovine serum (Gibco, Carlsbad, CA, USA). RAW 264.7 cells at a density of 1×10^6 cells/mL were seeded on the ECM-based scaffolds (Fig. 1C). RAW 264.7 cells were cultured on culture plates (TCP group) as a control. After overnight culture, 1 μg/ml lipopolysaccharide (Sigma-Aldrich, St Louis, MO, USA) was added to the medium followed by incubation for 2 h. Thereafter, the medium was changed to serum-free medium followed by incubation for another 6 h.

2.9. Gene expression analysis

Total RNA was isolated from the cell-scaffold composites biofabricated with or without mechanical loading on days 7, 14, and 21, and the ECM-based scaffolds treated with RAW 264.7 cells using an RNA extraction kit (TIANGEN, Beijing, China) according to the manufacturer's protocol. Total RNA was reverse transcribed into first-strand cDNA using SuperScript IV VILO Master Mix (Life Technologies, Carlsbad, CA, USA). qRT-PCR was performed using CFX96 Touch™ Real-Time PCR Detection System (Bio-Rad Laboratories, USA) via PowerUp™ SYBR™ Green Master Mix (Applied Biosystems A25742, USA). For the cell-scaffold composites biofabricated with or without mechanical loading, the expression levels of genes (*ALP, RUNX2, COL1A1, OCN, IL1B, TNFA, IL8, RANTES, GROa, PF4, and NAP2*) on days 7, 14 and 21 were examined; *ACTB* was used as the endogenous control, and relative gene expression for each gene was normalized to that of MSCs seeded on the scaffolds prior to mechanical loading, denoted as the Day 0 control. The expression levels of genes (*iNOS, Arg1, Cd80, Mrc1, Il1rn, Il1b, Il6, Tnf, Alpl, and Runx2*) were also determined in the macrophage polarization experiments; *Actb* was used as the endogenous control, and qRT-PCR data were normalized to the TCP control. The relative mRNA expression levels were analyzed using the $2^{-\Delta\Delta CT}$ method. All primer sequences are listed in Table 1.

2.10. Western blot analysis

To further assess the effect on macrophages polarization of the ECM-based scaffolds, the protein expression of iNOS (M1 marker) and Arg 1 (M2 marker) was measured by Western blot. In brief, total protein was extracted from RAW 264.7 cells using RIPA lysis buffer (Boster, Wuhan, China). The protein concentration was measured using a BCA protein assay kit (Boster, Wuhan, China). Proteins were electroblotted onto polyvinylidene difluoride membranes after sodium dodecyl sulfate-polyacrylamide gel electrophoresis. The membranes were then blocked with 5% skim milk and incubated with primary antibodies anti-iNOS (Bioss, Beijing, China), anti-Arg 1 (CST, Danvers, MA, USA), and anti-GAPDH (CST, Danvers, MA, USA) overnight at 4 °C. The membranes were rinsed three times in Tris-buffered-saline-Tween buffer before incubation with the appropriate secondary antibody (CST, Danvers, MA, USA) and then visualized using supersensitive luminescent liquid (Boster, Wuhan, China). The relative expression levels of proteins were determined by semiquantitative analysis using Image J software

Table 1
The sequences of primers used in the experiments.

Species	Gene	Primers	Sequences (5'to 3')
HUMAN	*IL1B*	Forward	TTTGAAGTTGACGGACCCCA
		Reverse	TGTTGATGTGCTGCTGCGAG
HUMAN	*TNFA*	Forward	GCTCCAGGCGGTGCTTGTTC
		Reverse	GGCTTGTCACTCGGGGTTCG
HUMAN	*IL8*	Forward	ACTGAGAGTGATTGAGAGTGGAC
		Reverse	AACCCTCTGCACCCAGTTTTC
HUMAN	*RANTES*	Forward	TGCTGCTTTGCCTACATTGCC
		Reverse	TCCTTGACCTGTGGACGACTGC
HUMAN	*GROa*	Forward	CAGGGAATTCACCCCAAGAACA
		Reverse	GGATGCAGGATTGAGGCAAGC
HUMAN	*PF4*	Forward	GGTCCGTCCCAGGCACATCA
		Reverse	TCTTCAGCGTGGCTATCAGTTGG
HUMAN	*NAP2*	Forward	GTAACAGTGCGAGACCACTTC
		Reverse	CTTTGCCTTTCGCCAAGTTTC
HUMAN	*ALP*	Forward	ACTGGGGCCTGAGATACCC
		Reverse	TCGTGTTGCACTGGTTAAAGC
HUMAN	*RUNX2*	Forward	ATCTCTACTATGGCACTTCGTCAGG
		Reverse	GCTTCCATCAGCGTCAACACC
HUMAN	*COL1A1*	Forward	AAGGTGTTGTGCGATGACG
		Reverse	GGCAGACGGGACAGCACT
HUMAN	*OCN*	Forward	CCTCACACTCCTCGCCCTATT
		Reverse	CTCCCAGCCATTGATACAGGT
HUMAN	*ACTB*	Forward	CAGGGCGTGATGGTGGGCA
		Reverse	CAAACATCATCTGGGTCATCTTCTC
MOUSE	*iNOS*	Forward	ACGGACGAGACGGATAGG
		Reverse	CGTGGGGTTGTTGCTGAA
MOUSE	*Arg1*	Forward	GTCAGTGTGGTGCTGGGTGG
		Reverse	TGGTTGTCAGGGGAGTGTTG
MOUSE	*Cd80*	Forward	TATTGCTGCCTTGCCGTTAC
		Reverse	TCCCAGCAATGACAGACAGC
MOUSE	*Mrc1*	Forward	GGTGGCTTATGGGATGTTTT
		Reverse	TTGGGTTCAGGAGTTGTTGT
MOUSE	*Il1rn*	Forward	TGTGCCAAGTCTGGAGATGA
		Reverse	GAGCGGATGAAGGTAAAGCG
MOUSE	*Il1b*	Forward	TTTGAAGTTGACGGACCCCA
		Reverse	TGTTGATGTGCTGCTGCGAG
MOUSE	*Il6*	Forward	GCCTTCTTGGGACTGATG
		Reverse	TCATTTCCACGATTTCCC
MOUSE	*Tnf*	Forward	TTCAAGGGACAAGGCTGC
		Reverse	ACGGCAGAGAGGAGGTTG
MOUSE	*Alpl*	Forward	AACCTGACTGACCCTTCGCT
		Reverse	TCAATCCTGCCTCCTTCCAC
MOUSE	*Runx2*	Forward	CAACAAGACCCTGCCCGT
		Reverse	ACAGCGGAGGCATTTCGG
MOUSE	*Actb*	Forward	GGCCAACCGTGAAAAGAT
		Reverse	GGCGTGAGGGAGAGCATA

All primers were purchased from TSINGKE Biological Technology Co,. LTD.

(NIH, Bethesda, MD).

2.11. In vivo bone regeneration of ECM-based scaffolds and micro-computed tomography (Micro-CT) analysis

A rabbit femoral condyle defect model (Fig. 1 D) for the assessment of bone regeneration was established, and the ECM-based scaffolds were implanted to evaluate the curative effect. Forty-two male New Zealand white rabbits with a body weight of 2.0–2.5 kg at 5 months of age were randomly divided into seven groups for the experiment: Blank scaffold group (n = 6), E-Loading-7d group (n = 6), E-Loading-14d group (n = 6), E-Loading-21d group (n = 6), E-Static-7d group (n = 6), E-Static-14d group (n = 6), and E-Static-21d group (n = 6). After anesthesia was induced, the rabbit was placed in the supine position on a special operating table, and the posterior legs were shaved and disinfected. Then a longitudinal incision was made on the lateral surface of each femoral condyle to expose the distal femur. A bone defect with a diameter of 4.5 mm and a depth of 10 mm was made using an orthopedic electric drill in the distal part of the rabbit femur, and ECM-based scaffolds or blank scaffolds were carefully implanted into the defects under strict aseptic conditions. Then, the incision was sutured layer by layer. Postoperatively antibiotics and analgesics were administered. The rabbits were euthanized with 5 mL/kg air after an intravenous injection of 30 mg/kg pentobarbital sodium for rabbits on Week 1 and Week 8 time points for sample collection. The femoral condyles were excised and stripped of soft tissue. The femoral condyles were then examined by Micro-CT (μCT100, Scanco Medical AG), and qualitative information on the ECM-based scaffolds was obtained by Micro-CT imaging using a microfocus X-ray CT system (SkyScan 1275, Germany) with a source voltage of 70 kV, source current of 200 μA and scanning resolution of 16.4 μm. A cylindrical area with 4.5 mm diameter of the ECM-based scaffold was selected as the region of interest (ROI) to assess newly formed bone. A threshold between 80 and 110 was applied to discriminate new bone from other tissues and the scaffold. The bone volume/total volume (BV/TV) in the ROI was utilized to estimate new bone formation using the software of the Micro-CT system based on 3D reconstructions.

2.12. Statistical analysis

Data with a Gaussian distribution were analyzed by unpaired *t*-test, and data with a non-Gaussian distribution were analyzed by a nonparametric (Mann-Whitney) test using GraphPad Prism 7.0 software (GraphPad, USA). Statistical significance was considered as $p < 0.05$.

3. Results

3.1. Differentiation capacity and immunophenotypical characteristics of hUCMSCs

Both alizarin red staining (Fig. 2A–B) and oil red O staining (Fig. 2C–D) illustrated significantly positive reactions. Immunophenotype detection by flow cytometry demonstrated the positive expression of MSC surface markers, including CD73, CD90, and CD105 (>95%, Fig. 2 E) and the negative expression of CD19, CD34, CD45, and HLA-DR (<2%, Fig. 2 F).

3.2. Effect of cyclic mechanical loading on cell viability and proliferation

The cell layers on the scaffold in the static groups showed significant detachment over time (Fig. 3C). In contrast, the porous surface of the scaffold in the mechanical loading groups was covered and filled by cell layers due to the massive expansion of MSCs on the scaffold (Fig. 3 D). Furthermore, as shown in Fig. 4A-B, Calcein-AM/PI staining also demonstrated that the cell viability in the mechanical loading groups was superior to that in the static groups on days 7, 14, and 21 ($p < 0.01$). The DNA content in the mechanical loading groups was significantly higher than that in the static groups at the predetermined time points (Fig. 4C, $p < 0.01$).

3.3. Effect of cyclic mechanical loading on proinflammatory and osteogenic biomarkers of MSCs seeded on scaffolds

The results of the Proteome Profiler Array showed that the expression of 26 of 31 proinflammatory proteins was decreased in the mechanical loading groups (Fig. 5A–B). Among these proteins, five proinflammatory proteins presented the most significantly increased expression in the static groups, including IL8, GROa, NAP2, PF4, and RANTES (Fig. 5 A).

The mRNA expression levels of *IL1B*, *IL8*, *NAP2*, *PF4*, and *RANTES* were downregulated in the mechanical loading groups (Fig. 6 A5, B2, B4, B5, B6). In the Loading-7d and Loading-21d groups, the mRNA expression of *TNFA* was downregulated (Fig. 6 B1). The mRNA expression of *GROa* in the Loading-14d group was downregulated (Fig. 6 B3). The mRNA expression of *ALP* (Loading-7d) and *RUNX2* (Loading-14d and Loading-21d groups) was significantly upregulated (Fig. 6 A1-A2). Furthermore, the gene expression of *COL1A1* was upregulated in the Loading-14d and Loading-21d groups (Fig. 6 A4).

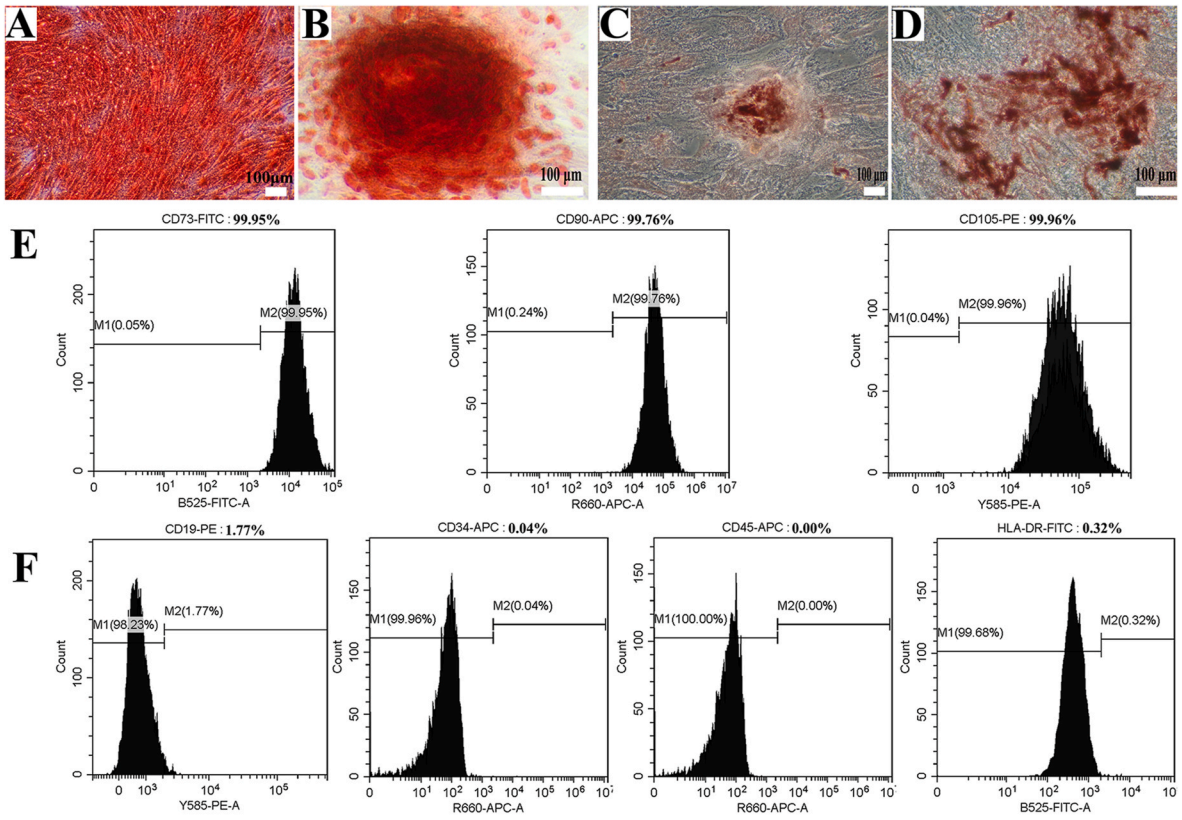

Fig. 2. Characteristics of hUCMSCs. **A-D)** Osteogenic (**A-B**, Alizarin red staining) and adipogenic (**C-D**, Oil red O staining) differentiation identification after 3 weeks of induction culture. Scale bars = 100 μm. **E-F)** Identification of MSCs immunophenotype by flow cytometry (positive biomarkers including CD73, CD90, and CD105; negative biomarkers including CD19, CD34, CD45, and HLA-DR).

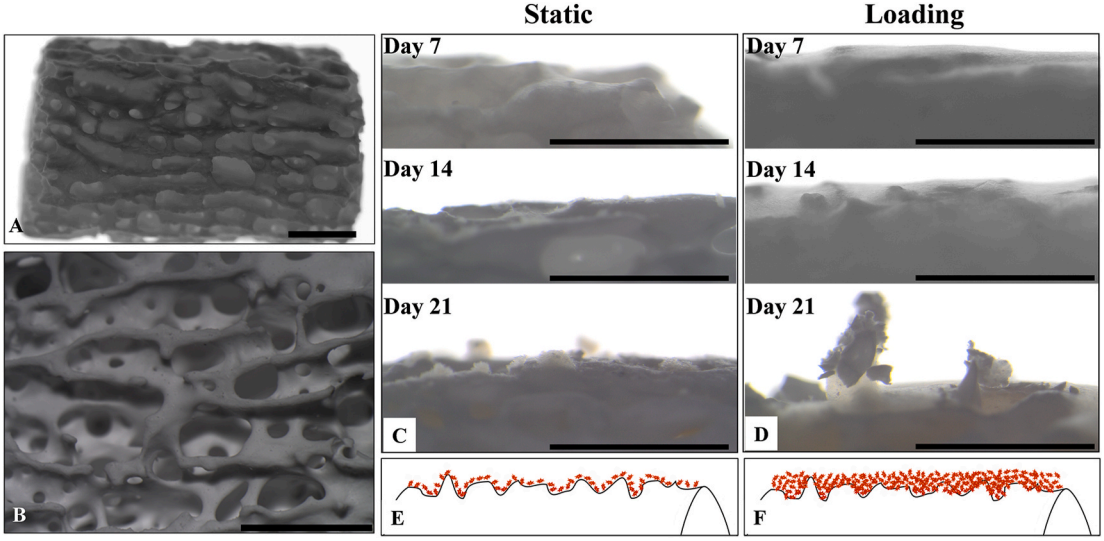

Fig. 3. Gross view under the stereomicroscope. **A-B)** 3D porous structure of calcined bovine bone scaffold. **C)** Dynamic change of cellular layers on the scaffold surface after being cultured statically for 7, 14, and 21 days. **D)** Dynamic change of cellular layers on the scaffold surface after being cultured by mechanical loading for 7, 14, and 21 days. **E)** Illustration of cell growth on the scaffold surface in the static groups. **F)** Illustration of cell growth on the scaffold surface in the mechanical loading groups. Scale bars = 2000 μm.

3.4. Effect of ECM-based scaffolds on macrophage polarization

The expression of macrophage polarization-related genes was then investigated by qRT-PCR. The expression of *iNOS* (Fig. 7 A1), acting as a M1-related marker, was downregulated in the E-Loading-7d, E-Loading-14d, and E-Loading-21d groups. The expression of *Cd80* (Fig. 7 A2), acting as a M1-related marker, was downregulated in the E-Loading-14d and E-Loading-21d groups.

In contrast, *Il1rn* (anti-inflammatory marker), *Arg1* and *Mrc1* (M2-related markers), and *Alpl* and *Runx2* (bone regeneration-related markers) expression was upregulated (Fig. 7 B3, B1, B2, B4, B5) in the E-Loading-7d, E-Loading-14d, and E-Loading-21d groups. *Il1b*

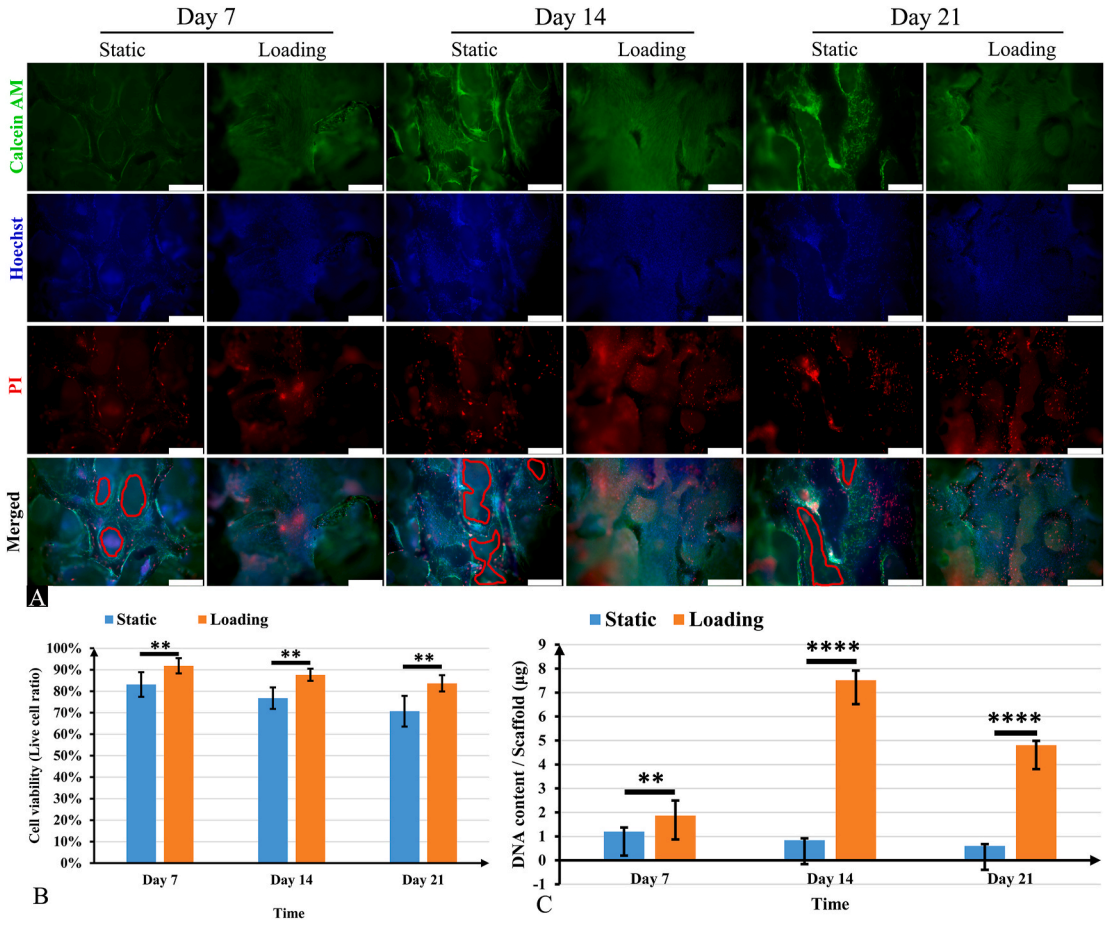

Fig. 4. Calcein AM/PI/Hoechst cell staining and the DNA quantification of cell-scaffold composite. **A)** Cell-scaffold composites were stained with Calcein AM, PI and Hoechst after being cultured statically or dynamically for 7, 14, and 21 days; MSCs seeded on scaffold did not achieve complete cellular confluence in the static groups (red circles). (Scale bars = 500 μm, n = 3). **B)** Cell viability assessment by comparing the live cell ratio (n = 3, Mean ± SD, $^{**}p < 0.01$). **C)** DNA quantification per scaffold in different groups (n = 6, Mean ± SD, $^{**}p < 0.01$, $^{****}p < 0.0001$).

(proinflammatory marker) (Fig. 7 A3) expression was significantly downregulated in the E-Loading-7d, E-Loading-14d, and E-Loading-21d groups. Additionally, the protein expression of Arg 1 was upregulated (Fig. 8) in the E-Loading-7d, E-Loading-14d, and E-Loading-21d groups, while the protein expression of iNOS was downregulated in the E-Loading-21d group (Fig. 8).

3.5. Efficacy of ECM-based scaffolds in bone defect repair in vivo

3D CT reconstruction images were observed and BV/TV ratio were used to assess the newly formed bone tissues. One week after implantation, 3D CT reconstruction images did not show new formation bone tissue in all treated groups (data no shown). After eight weeks of implantation, the experimental results showed a little of new bone formation (BV/TV: 12.23 ± 3.80%) in the 3D CT reconstruction image for the blank scaffold group (Fig. 9 A) compared with other experimental groups. On the other hand, 3D CT reconstruction results in the experimental groups showed that the porous area of the scaffolds was gradually filling with new bone tissues that was similar to the normal bone (BV/TV: Fig. 9 B 19.72 ± 4.62%; Fig. 9C 22.29 ± 7.20%; Fig. 9 D 19.23 ± 3.00%; Fig. 9 E 22.28 ± 3.02%; Fig. 9 F 20.85 ± 2.03%; Fig. 9 G 32.95 ± 2.89%). Moreover, BV/TV qualitative results (Fig. 9H) displayed that the percentage of neonatal bone mass in the E-Loading-21d group was higher compared with E-Static-21d group (20.85 ± 2.03% vs 32.95 ± 2.89%, $p < 0.01$).

4. Discussion

Mechanical stimuli to most bone tissues in vivo are dynamic, which indicates that these tissues are under loading and resting cycles [14]. Thus, cyclic mechanical stimuli should not be neglected during the biofabrication of hydroxyapatite scaffolds for bone regeneration. The present study shows that mechanical stimuli helped to alleviate the inflammatory responses and enhance the osteogenesis of MSCs seeded on 3D scaffolds. Moreover, ECM-based scaffolds facilitated the polarization of macrophages from a proinflammatory phenotype (M1) toward an anti-inflammatory phenotype (M2) in vitro in a manner that was dependent on whether the cell-scaffold composites were initially biofabricated under mechanical loading or static culture conditions. Furthermore, the ECM-based scaffolds that were biofabricated with mechanical loading before freeze-drying promoted new bone formation in vivo.

The excessive expression of proinflammatory mediators has a negative effect on bone regeneration. IL1B and TNFA significantly suppress the osteogenic differentiation of MSCs [40–42]. Moreover, the levels of inflammatory cytokines, such as IL1B and TNFA, could affect the outcome of bone regeneration at bone fracture or defect sites treated with exogenous BMP-2 [43]. However, bone tissue regeneration is enhanced by inhibiting the synthesis of inflammatory mediators such as IL1B, IL6, IL8, and TNFA [44–46]. In the present study, the expression of proinflammatory mediators (*IL1B*, IL8, and *TNFA*), except for the gene expression of *TNFA* on day 14, was reduced in the mechanical loading groups, which may have a positive impact on improving the

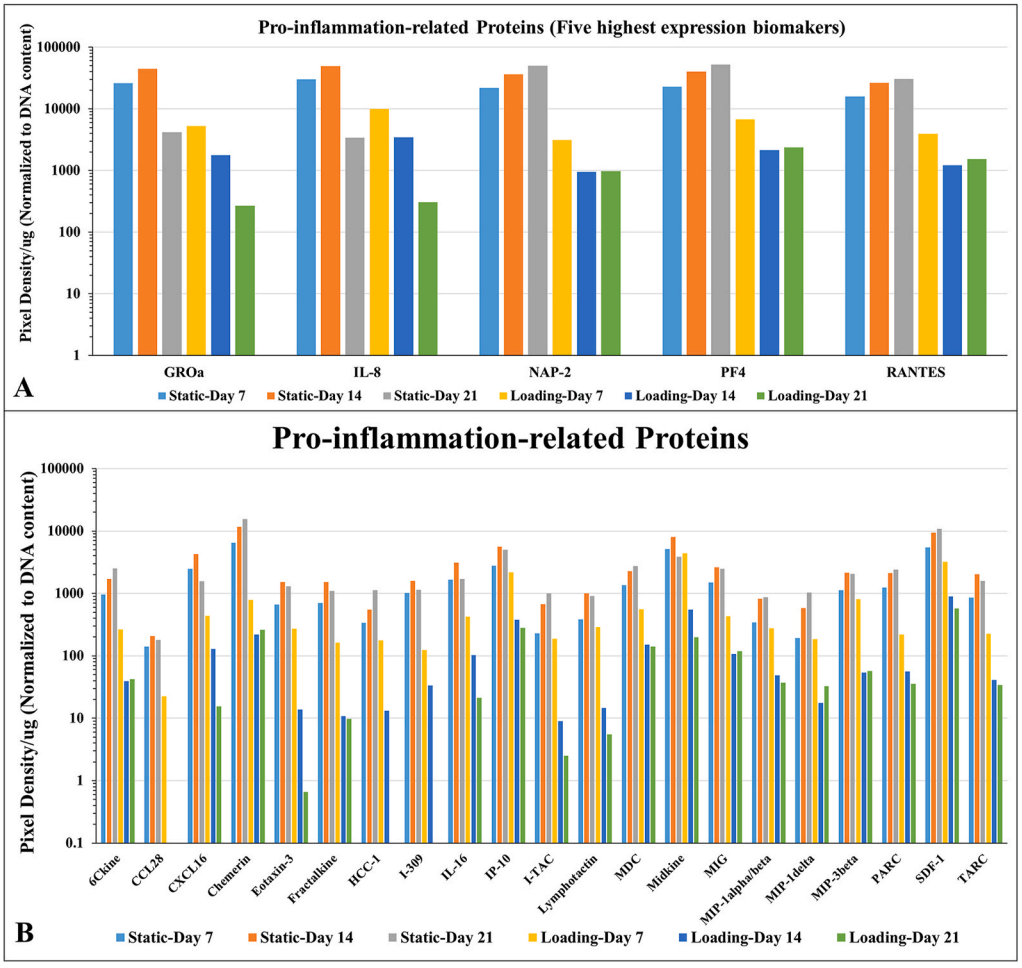

Fig. 5. Screening of proinflammatory proteins by Proteome Profiler Array (n = 1). **A)** Five proinflammatory proteins presented the most significantly increased expression at the 7th, 14th, and 21st day in the static groups. **B)** Alterations of other proinflammatory proteins at the 7th, 14th, and 21st day in the mechanical loading or the static groups. Data were normalized to the DNA content of corresponding group. The five proteins with the highest expression were further analyzed by qRT-PCR.

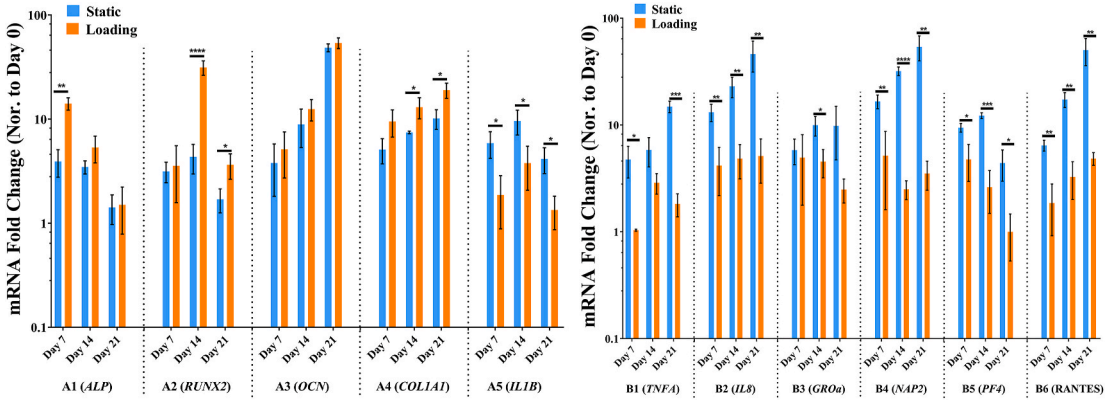

Fig. 6. The expression of osteogenic **(A1-A4)** and proinflammatory **(A5, B1–B5)** genes of MSCs seeded on scaffolds in the mechanical loading or the static groups. n = 3, Mean ± SD; *$p < 0.05$, **$p < 0.01$, ***$p < 0.001$, ****$p < 0.001$; *ALP*: Alkaline phosphatase, *COL1A1*: Collagen 1A1, *RUNX2*: Runt-related transcription factor 2, *OCN*: Osteocalcin, *IL*: Interleukin, *TNF*A: Tumor necrosis factor alpha, *GROa*: Growth-regulated oncogene alpha, *NAP2*: Neutrophile-activating protein 2, *PF4*: Platelet factor 4, *RANTES*: regulated upon activation normal T cell expressed and secreted.

osteogenesis induced by bone regenerative biomaterials.

On the other hand, some chemokines (GROα, PF4, NAP2, and RANTES) are considered to be important components of proinflammatory mediators and to interfere with the process of tissue regeneration [47–49]. As shown in Fig. 5 A-B and Fig.6, the expression of these mediators was obviously suppressed on days 7, 14 and 21 at the gene and protein levels by mechanical loading, except for the gene expression of *GROα* on days 7 and 21. This further confirmed that mechanical loading alleviated the inflammatory response of MSCs seeded on the scaffold.

Previously, using dynamic compression to investigate the effects of ECM deformations on the regulation of angiogenesis during bone tissue regeneration, Ruehle et al. found that the expression of inflammation-related genes (*Cxcl 12, Tnf*) was significantly downregulated and the expression of regeneration-related genes (*Bmp2, Col 1a1* and *Vegfa*) was upregulated by mechanical loading [50]. Mechanical stimuli also

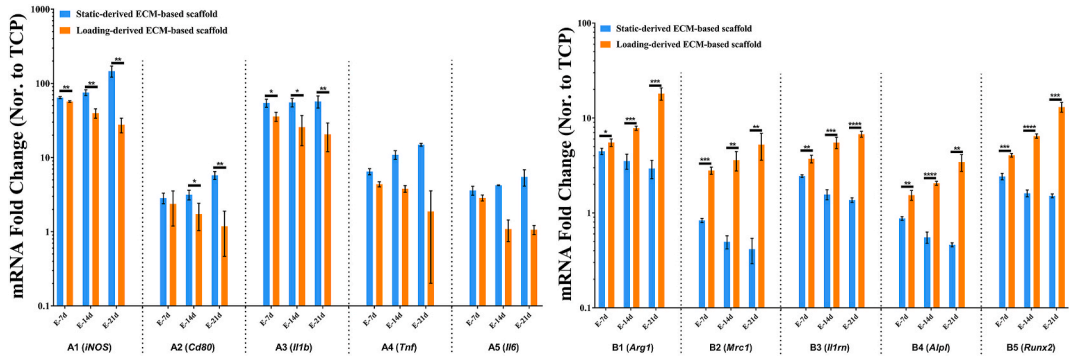

Fig. 7. The expression levels of macrophage polarization-related genes induced by ECM-based scaffolds. **A1-A2)** M1 marker genes. **A3-A5)** proinflammatory genes. **B1–B2)** M2 marker genes. **B3)** anti-inflammatory gene. **B4–B5)** bone regeneration-related genes. n = 3, Mean ± SD; $*p < 0.05$, $**p < 0.01$, $***p < 0.001$, $****p < 0.001$; Arg 1: Arginase 1, iNOS: Inducible nitric oxide synthase. E−7d: ECM-based scaffolds from E-Static- or E-Loading-7d group; E−14d: ECM-based scaffolds from E-Static- or E-Loading-14d group; E−21d: ECM-based scaffolds from E-Static- or E-Loading-21d group. Static-derived ECM-based scaffolds: the ECM-based scaffolds that were prepared with static culture before freeze-drying; Loading-derived ECM-based scaffolds: the ECM-based scaffolds that were biofabricated with mechanical loading before freeze-drying.

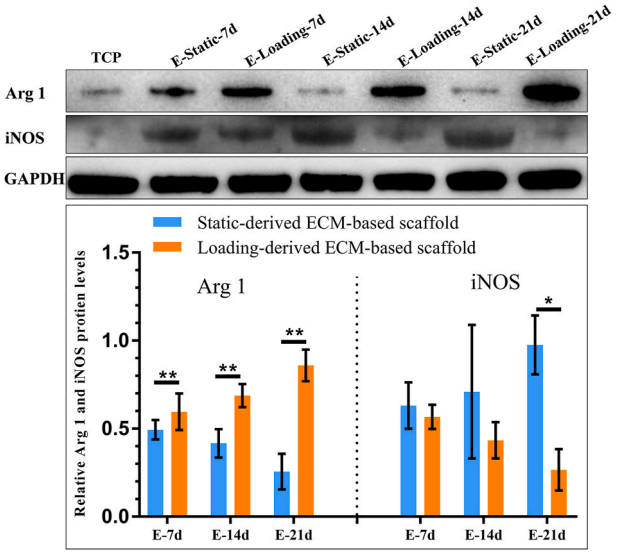

Fig. 8. Western blot and semi-quantitative analysis of macrophage polarization-related proteins induced by ECM-based scaffolds. The expression of Arg 1 (M2 marker protein) and iNOS (M1 marker protein) after co-culture of ECM-based scaffolds and macrophages. n = 3, Mean ± SD; $*p < 0.05$, $**p < 0.01$.

provide critical cues for MSCs residing at the vascular interface in terms of the effects of antioxidation and anti-inflammation [51]. Angelina et al. reported that mechanical loading could regulate the characteristics of polycaprolactone nanofiber substrates and accelerate tendon repair by reducing proinflammatory responses both in vitro and in vivo [52]. Although these studies did not directly demonstrate that mechanical stimuli ameliorated the inflammatory response of MSCs on bone biomaterials, mechanical stimuli played a critical role in cellular inflammatory modulation, as shown in the present study.

Taken together, the results of this study demonstrate that the inflammatory response of MSCs could be modulated by mechanical stimuli. The mechanical microenvironment could be considered a biofabrication strategy to develop bone biomaterials with low immunoinflammatory properties.

ECM-based biomaterials for bone regeneration could mimic the 3D architecture and bioactive components of bone to foster cell proliferation, recruitment, and osteogenic differentiation. Mechanical stimuli are beneficial for the osteogenic differentiation of MSCs [53–55] and local ECM deposition within MSC-seeded biomaterials [56,57]. In the present study, cyclic mechanical loading in hydroxyapatite scaffold biofabrication somewhat mimicked the complex 3D in vivo microenvironment of bone tissue. The natural hydroxyapatite scaffolds that were fabricated from calcined bovine vertebral cancellous bone mimicked the hydroxyapatite composition and internal 3D architecture of human bone. The expression of the key genes for early osteogenesis in the mechanical loading groups, *ALP* (day 7) and *RUNX2* (days 14 and 21), was significantly upregulated compared with that of genes in the static groups. The expression of the bone mineralization marker *COL1A1* in the mechanical loading groups was also obviously upregulated on days 14 and 21. Meanwhile, applying mechanical stimuli to MSCs seeded on the scaffolds promoted cellular proliferation and improved cellular viability. Additionally, in vivo experiments further demonstrated that the ECM-based scaffolds that were biofabricated with mechanical loading for 21 days before freeze-drying promoted new bone formation (BV/TV, E-Static-21d group vs E-loading-21d group: 20.85 ± 2.03% vs 32.95 ± 2.89%, $p < 0.01$). These results showed that mechanical stimuli enhanced the osteogenic differentiation, proliferation, and viability of MSCs seeded on the scaffold, which is in line with the results of other studies [24,53,58,59]. Thus, applying mechanical stimuli as a biofabrication approach for developing tissue-engineered bone grafts could overcome some of the drawbacks of traditional bone tissue engineering techniques.

For bone regeneration biomaterials, another issue of concern is that an acceptable immunoinflammatory response induced by biomaterials plays a vital role in realizing the tissue repair process [60]. It is an important strategy to use the functional phenotypes of macrophages activated by biomaterials to assess the regenerative and immunoregulatory potential of biomaterials [7,61,62]. Based on the phenotypical and functional stability of the RAW264.7 murine macrophage line [63,64], an inflammatory model was established by activating RAW264.7 cells with 1 μg/ml lipopolysaccharide to preliminarily evaluate the immunoinflammatory properties of the ECM-based scaffolds. The results showed that the ECM-based scaffolds that were biofabricated with mechanical loading before freeze-drying facilitated anti-inflammatory and regenerative macrophage polarization toward M2 phenotype compared with static groups on days 7, 14, and 21, which also verified the potential effect of mechanical stimuli on modulating the immunoinflammatory property of bone regenerative biomaterials.

There are three major limitations to this study that could be addressed in future research. First, the inflammatory response estimates in this study are based on in vitro experiments. As reported from a multicenter analysis [65], there is a surprisingly poor correlation between the results of in vitro and in vivo testing of biomaterials for bone

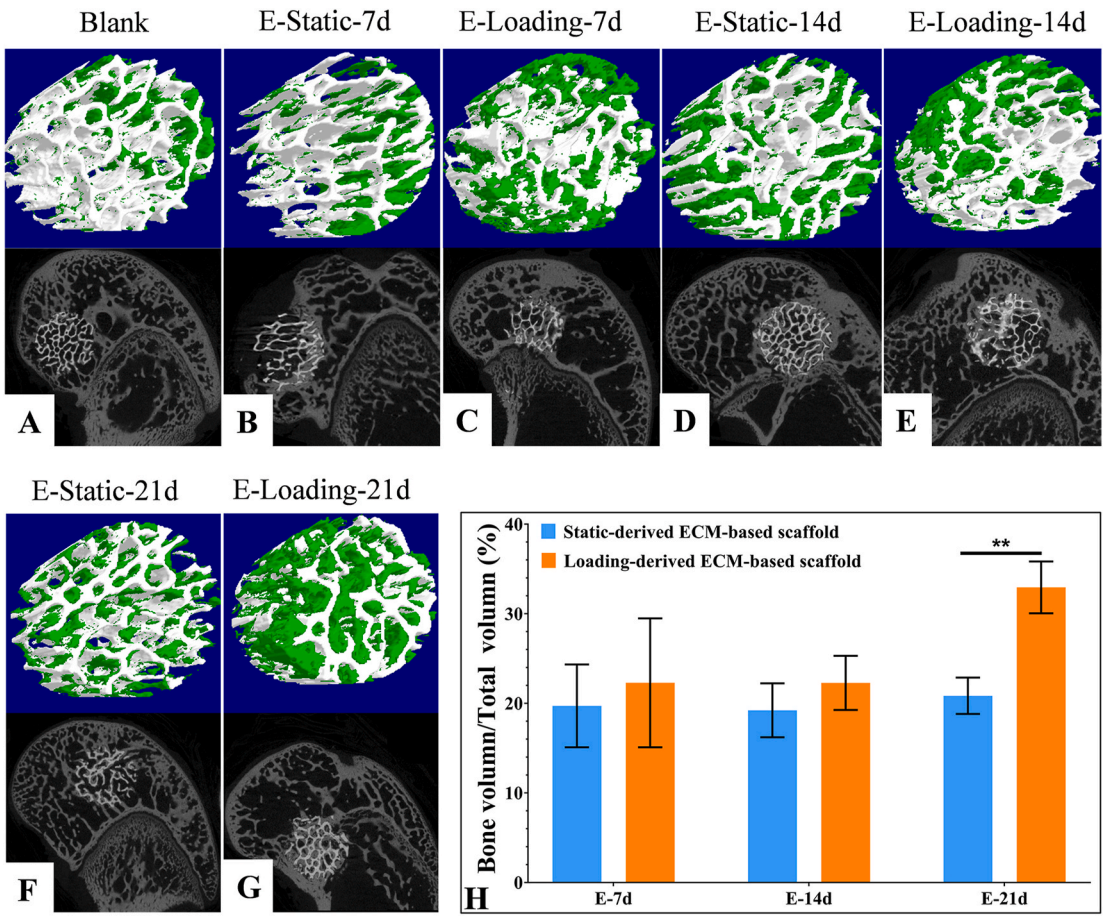

Fig. 9. Repairment of rabbit bone defects in vivo. **A-G)** Micro-CT 3D reconstruction of in vivo new bone formation (green area) ability of the blank scaffold (white area) group and ECM-based scaffolds (white area) after 8 weeks of implanatation. **H)** Quantitative analysis of bone volume/total volume (BV/TV) of ECM-based scaffolds after implanted in vivo for 8 weeks based on the Micro-CT evaluation. n = 3, Mean ± SD; $^{**}p < 0.01$.

regeneration. To overcome the inadequacies of the lack of an immune response for in vitro assessments of osteogenesis, a novel in vitro approach to verify biomaterial related properties before preclinical studies was applied in this study. Herein, as a strategy of concern to evaluate the osteoimmunomodulatory effect of biomaterials [7], an in vitro macrophage polarization model was used to assess the inflammatory response induced by the ECM-based scaffolds. The results confirmed the low inflammatory response induced by the ECM-based scaffolds that were biofabricated with mechanical loading before freeze-drying. Further study is warranted to investigate the in vivo inflammatory responses and macrophage polarization induced by ECM-based scaffolds by histological analysis. Second, previous studies on cellular fates under compressive mechanical loading have shown inconsistent conclusions [57,59,66] due to differences in the bioreactor parameters, cell types and biomaterials. Therefore, comparing various mechanical loading modes will help to comprehensively elucidate the biological effects of mechanical stimuli on cell-scaffold composites in further studies. Third, the mechanical loading stress produced by the bioreactor could not be fully applied to the cell-scaffold composites in the expected linear wave mode due to the natural calcined scaffold having the properties of relative rigidity, brittleness, and a non-absolute cylindrical shape.

5. Conclusions

The mechanical microenvironment derived from cyclic mechanical loading, as a biofabrication strategy for bone regenerative biomaterials, could have dual efficacy in modulating the inflammatory microenvironment and stimulating the osteogenic differentiation of MSCs seeded on 3D scaffolds by suppressing the expression of inflammatory biomarkers and enhancing the expression of osteogenic biomarkers. The ECM-based scaffolds that were biofabricated with mechanical loading before freeze-drying facilitated the M2 polarization of macrophages in vitro and new bone formation in vivo, which verified the low inflammatory response and regenerative capability of the scaffolds.

Declaration of competing interest

The authors declare no conflict of interest.

CRediT authorship contribution statement

Penghui Zhang: Methodology, Formal analysis, Investigation, Writing – original draft. **Xizhe Liu:** Investigation, Writing – review & editing. **Peng Guo:** Formal analysis, Investigation, Writing – original draft. **Xianlong Li:** Validation, Investigation. **Zhongyuan He:** Investigation. **Zhen Li:** Conceptualization, Writing – review & editing. **Martin J. Stoddart:** Conceptualization, Writing – review & editing. **Sibylle Grad:** Conceptualization, Writing – review & editing. **Wei Tian:** Visualization, Funding acquisition. **Dafu Chen:** Conceptualization, Project administration, Funding acquisition. **Xuenong Zou:** Conceptualization, Writing – review & editing, Visualization, Funding acquisition. **Zhiyu Zhou:** Conceptualization, Data curation, Writing – review & editing, Supervision, Project administration, Funding acquisition. **Shaoyu Liu:** Conceptualization, Resources, Supervision, Project administration,

Funding acquisition.

Acknowledgments

This research was supported by the National Natural Science Foundation of China (Grant no. 32071351, 81772400 and 31900583, 32071341), the Fundamental Research Funds for the Central Universities (Grant no. 19ykzd05), the Committee for Science and Technology Innovation of Shenzhen (Grant no. JCYJ20190809142211354 and GJHZ20180929160004704), the Sanming Project of Medicine in Shenzhen (Grant no. SZSM201911002), the Natural Science Foundation of Guangzhou City (Grant no. 201807010031, 201704030082), and the Beijing Municipal Health Commission (Grant no. BMHC-2019-9; BMHC-2018-4; PXM2020_026275_000002).

References

[1] R.J. O'Keefe, et al., Bone tissue engineering and regeneration: from discovery to the clinic–an overview, Tissue Eng. B Rev. 17 (2011) 389–392, https://doi.org/10.1089/ten.TEB.2011.0475.
[2] A. Ho-Shui-Ling, et al., Bone regeneration strategies: engineered scaffolds, bioactive molecules and stem cells current stage and future perspectives, Biomaterials 180 (2018) 143–162, https://doi.org/10.1016/j.biomaterials.2018.07.017.
[3] T.F. Putters, et al., Morbidity of anterior iliac crest and calvarial bone donor graft sites: a 1-year randomized controlled trial, Int. J. Oral Maxillofac. Surg. 47 (2018) 1474–1480, https://doi.org/10.1016/j.ijom.2018.06.002.
[4] K.S. Boehm, et al., Donor site morbidities of iliac crest bone graft in craniofacial surgery: a systematic review, Ann. Plast. Surg. 83 (2019) 352–358, https://doi.org/10.1097/SAP.0000000000001682.
[5] S.N. Parikh, et al., Bone graft substitutes: past, present, future, J. Postgrad. Med. 48 (2002) 142–148.
[6] O. Veiseh, et al., Size- and shape-dependent foreign body immune response to materials implanted in rodents and non-human primates, Nat. Mater. 14 (2015) 643–651, https://doi.org/10.1038/nmat4290.
[7] Z. Chen, et al., Tuning chemistry and topography of nanoengineered surfaces to manipulate immune response for bone regeneration applications, ACS Nano 11 (2017) 4494–4506, https://doi.org/10.1021/acsnano.6b07808.
[8] J.M. Sadowska, et al., Effect of nano-structural properties of biomimetic hydroxyapatite on osteoimmunomodulation, Biomaterials 181 (2018) 318–332, https://doi.org/10.1016/j.biomaterials.2018.07.058.
[9] J.Y. Lee, et al., Design of a 3D BMP-2-delivering tannylated PCL scaffold and its anti-oxidant, anti-inflammatory, and osteogenic effects in vitro, Int. J. Mol. Sci. 19 (2018), https://doi.org/10.3390/ijms19113602.
[10] A.H. Lourenco, et al., Osteogenic, anti-osteoclastogenic and immunomodulatory properties of a strontium-releasing hybrid scaffold for bone repair, Mater Sci Eng C Mater Biol Appl 99 (2019) 1289–1303, https://doi.org/10.1016/j.msec.2019.02.053.
[11] C. Dai, et al., Three-dimensional high-porosity chitosan/honeycomb porous carbon/hydroxyapatite scaffold with enhanced osteoinductivity for bone regeneration, ACS Biomater Sci Eng 6 (2019) 575–586.
[12] X. Zhang, et al., Novel hierarchical nitrogen-doped multiwalled carbon nanotubes/cellulose/nanohydroxyapatite nanocomposite as an osteoinductive scaffold for enhancing bone regeneration, ACS Biomater Sci Eng 5 (2018) 294–307.
[13] I.G. Kim, et al., Bioactive cell-derived matrices combined with polymer mesh scaffold for osteogenesis and bone healing, Biomaterials 50 (2015) 75–86, https://doi.org/10.1016/j.biomaterials.2015.01.054.
[14] G. Huang, et al., Functional and biomimetic materials for engineering of the three-dimensional cell microenvironment, Chem. Rev. 117 (2017) 12764–12850, https://doi.org/10.1021/acs.chemrev.7b00094.
[15] H. Lu, et al., Cultured cell-derived extracellular matrix scaffolds for tissue engineering, Biomaterials 32 (2011) 9658–9666, https://doi.org/10.1016/j.biomaterials.2011.08.091.
[16] T. Long, et al., Fabrication of three-dimensional porous scaffold based on collagen fiber and bioglass for bone tissue engineering, J. Biomed. Mater. Res. B Appl. Biomater. 103 (2015) 1455–1464, https://doi.org/10.1002/jbm.b.33328.
[17] R.X. Wu, et al., Modulating macrophage responses to promote tissue regeneration by changing the formulation of bone extracellular matrix from filler particles to gel bioscaffolds, Mater Sci Eng C Mater Biol Appl 101 (2019) 330–340, https://doi.org/10.1016/j.msec.2019.03.107.
[18] M.S. Carvalho, et al., Co-culture cell-derived extracellular matrix loaded electrospun microfibrous scaffolds for bone tissue engineering, Mater Sci Eng C Mater Biol Appl 99 (2019) 479–490, https://doi.org/10.1016/j.msec.2019.01.127.
[19] I.G. Kim, et al., Mechanotransduction of human pluripotent stem cells cultivated on tunable cell-derived extracellular matrix, Biomaterials 150 (2018) 100–111, https://doi.org/10.1016/j.biomaterials.2017.10.016.
[20] J. Ma, et al., Biomimetic matrix fabricated by LMP-1 gene-transduced MC3T3-E1 cells for bone regeneration, Biofabrication 9 (2017), 045010, https://doi.org/10.1088/1758-5090/aa8dd1.
[21] J.L. Milan, et al., Computational modelling of the mechanical environment of osteogenesis within a polylactic acid-calcium phosphate glass scaffold, Biomaterials 30 (2009) 4219–4226, https://doi.org/10.1016/j.biomaterials.2009.04.026.
[22] T.M. Skerry, et al., The response of bone to mechanical loading and disuse: fundamental principles and influences on osteoblast/osteocyte homeostasis, Arch. Biochem. Biophys. 473 (2008) 117–123, https://doi.org/10.1016/j.abb.2008.02.028.
[23] N. Kimelman-Bleich, et al., The effect of ex vivo dynamic loading on the osteogenic differentiation of genetically engineered mesenchymal stem cell model, J Tissue Eng Regen Med 5 (2011) 384–393, https://doi.org/10.1002/term.324.
[24] M. Jagodzinski, et al., Influence of perfusion and cyclic compression on proliferation and differentiation of bone marrow stromal cells in 3-dimensional culture, J. Biomech. 41 (2008) 1885–1891, https://doi.org/10.1016/j.jbiomech.2008.04.001.
[25] A. Ravichandran, , et al.In v, Itro cyclic compressive loads potentiate early osteogenic events in engineered bone tissue, J. Biomed. Mater. Res. B Appl. Biomater. 105 (2017) 2366–2375, https://doi.org/10.1002/jbm.b.33772.
[26] Z. Kong, et al., Dynamic compression promotes proliferation and neovascular networks of endothelial progenitor cells in demineralized bone matrix scaffold seed, J. Appl. Physiol. 113 (1985) 619–626, https://doi.org/10.1152/japplphysiol.00378.2011.
[27] A. Ruggiu, et al., Bone mechanobiology, gravity and tissue engineering: effects and insights, J Tissue Eng Regen Med 9 (2015) 1339–1351, https://doi.org/10.1002/term.1942.
[28] F. Guilak, et al., Biomechanics and mechanobiology in functional tissue engineering, J. Biomech. 47 (2014) 1933–1940, https://doi.org/10.1016/j.jbiomech.2014.04.019.
[29] V. David, et al., Ex Vivo bone formation in bovine trabecular bone cultured in a dynamic 3D bioreactor is enhanced by compressive mechanical strain, Tissue Eng. 14 (2008) 117–126, https://doi.org/10.1089/ten.a.2007.0051.
[30] J.J. Pfannkuche, et al., Intervertebral disc organ culture for the investigation of disc pathology and regeneration - benefits, limitations, and future directions of bioreactors, Connect. Tissue Res. 61 (2020) 304–321, https://doi.org/10.1080/03008207.2019.1665652.
[31] D.F. Williams, et al., On the mechanisms of biocompatibility, Biomaterials 29 (2008) 2941–2953, https://doi.org/10.1016/j.biomaterials.2008.04.023.
[32] Y. Liu, et al., Mesenchymal stem cell-based tissue regeneration is governed by recipient T lymphocytes via IFN-gamma and TNF-alpha, Nat. Med. 17 (2011) 1594–1601, https://doi.org/10.1038/nm.2542.
[33] A.G. Solis, et al., Mechanosensation of cyclical force by PIEZO1 is essential for innate immunity, Nature 573 (2019) 69–74, https://doi.org/10.1038/s41586-019-1485-8.
[34] J. Albarran-Juarez, et al., Piezo1 and Gq/G11 promote endothelial inflammation depending on flow pattern and integrin activation, J. Exp. Med. 215 (2018) 2655–2672, https://doi.org/10.1084/jem.20180483.
[35] C. Qiao, et al., Human mesenchymal stem cells isolated from the umbilical cord, Cell Biol. Int. 32 (2008) 8–15, https://doi.org/10.1016/j.cellbi.2007.08.002.
[36] B. Gantenbein, et al., An in vitro organ culturing system for intervertebral disc explants with vertebral endplates: a feasibility study with ovine caudal discs, Spine (Phila Pa 31 (1976) 2665–2673, https://doi.org/10.1097/01.brs.0000244620.15386.df.
[37] S. Illien-Junger, et al., The combined effects of limited nutrition and high-frequency loading on intervertebral discs with endplates, Spine (Phila Pa 35 (1976) 1744–1752, https://doi.org/10.1097/BRS.0b013e3181c48019.
[38] M. Brunelli, et al., Short bursts of cyclic mechanical compression modulate tissue formation in a 3D hybrid scaffold, J Mech Behav Biomed Mater 71 (2017) 165–174, https://doi.org/10.1016/j.jmbbm.2017.03.008.
[39] M. Shariatzadeh, et al., Effect of mechanical loading on osteogenesis of human embryonic stem cell-derived mesenchymal progenitors within collagen microspheres, J. Cell Sci. Ther. 9 (2018), https://doi.org/10.4172/2157-7013.1000282.
[40] K. Hu, et al., Long noncoding RNA ZBED3-AS1 induces the differentiation of mesenchymal stem cells and enhances bone regeneration by repressing IL-1beta via Wnt/beta-catenin signaling pathway, J. Cell. Physiol. 234 (2019) 17863–17875, https://doi.org/10.1002/jcp.28416.
[41] D.C. Lacey, et al., Proinflammatory cytokines inhibit osteogenic differentiation from stem cells: implications for bone repair during inflammation, Osteoarthritis Cartilage 17 (2009) 735–742, https://doi.org/10.1016/j.joca.2008.11.011.
[42] M.M. Martino, et al., Inhibition of IL-1R1/MyD88 signalling promotes mesenchymal stem cell-driven tissue regeneration, Nat. Commun. 7 (2016) 11051, https://doi.org/10.1038/ncomms11051.
[43] R.L. Huang, et al., Opposing TNF-alpha/IL-1beta- and BMP-2-activated MAPK signaling pathways converge on Runx2 to regulate BMP-2-induced osteoblastic differentiation, Cell Death Dis. 5 (2014) e1187, https://doi.org/10.1038/cddis.2014.101.
[44] J.D. Glaeser, et al., Anti-inflammatory peptide attenuates edema and promotes BMP-2-induced bone formation in spine fusion, Tissue Eng. 24 (2018) 1641–1651, https://doi.org/10.1089/ten.TEA.2017.0512.
[45] S.M. Barbalho, et al., The potential role of medicinal plants in bone regeneration, Alternative Ther. Health Med. 25 (2019) 32–39.
[46] I. Fasolino, et al., Osteoinductive and anti-inflammatory properties of chitosan-based scaffolds for bone regeneration, Mater Sci Eng C Mater Biol Appl 105 (2019) 110046, https://doi.org/10.1016/j.msec.2019.110046.
[47] L. Gao, et al., Decellularized aortic scaffold alleviates H2O2-induced inflammation and apoptosis in CD34+ progenitor cells while driving neovasculogenesis, BioMed Res. Int. (2020) 6782072, https://doi.org/10.1155/2020/6782072.

[48] C. Bakogiannis, et al., Platelet-derived chemokines in inflammation and atherosclerosis, Cytokine 122 (2019) 154157, https://doi.org/10.1016/j.cyto.2017.09.013.
[49] H.E. Broxmeyer, et al., Comparative analysis of the human macrophage inflammatory protein family of cytokines (chemokines) on proliferation of human myeloid progenitor cells. Interacting effects involving suppression, synergistic suppression, and blocking of suppression, J. Immunol. 150 (1993) 3448–3458.
[50] M.A. Ruehle, et al., Extracellular matrix compression temporally regulates microvascular angiogenesis, Sci. Adv. 6 (2020) eabb6351, https://doi.org/10.1126/sciadv.abb6351.
[51] M.F. Diaz, et al., Biomechanical forces promote immune regulatory function of bone marrow mesenchymal stromal cells, Stem Cell. 35 (2017) 1259–1272, https://doi.org/10.1002/stem.2587.
[52] A.D. Schoenenberger, et al., Macromechanics and polycaprolactone fiber organization drive macrophage polarization and regulate inflammatory activation of tendon in vitro and in vivo, Biomaterials 249 (2020) 120034, https://doi.org/10.1016/j.biomaterials.2020.120034.
[53] J. Ji, et al., The effect of mechanical loading on osteogenesis of human dental pulp stromal cells in a novel in vitro model, Cell Tissue Res. 358 (2014) 123–133, https://doi.org/10.1007/s00441-014-1907-8.
[54] K.T. Shalumon, et al., Rational design of gelatin/nanohydroxyapatite cryogel scaffolds for bone regeneration by introducing chemical and physical cues to enhance osteogenesis of bone marrow mesenchymal stem cells, Mater Sci Eng C Mater Biol Appl 104 (2019) 109855, https://doi.org/10.1016/j.msec.2019.109855.
[55] C.B. Horner, et al., Spatially regulated multiphenotypic differentiation of stem cells in 3D via engineered mechanical gradient, ACS Appl. Mater. Interfaces 11 (2019) 45479–45488, https://doi.org/10.1021/acsami.9b17266.
[56] M.G. Haugh, et al., Temporal and spatial changes in cartilage-matrix-specific gene expression in mesenchymal stem cells in response to dynamic compression, Tissue Eng. 17 (2011) 3085–3093, https://doi.org/10.1089/ten.tea.2011.0198.
[57] N. Sawatjui, et al., Biomimetic scaffolds and dynamic compression enhance the properties of chondrocyte- and MSC-based tissue-engineered cartilage, J Tissue Eng Regen Med 12 (2018) 1220–1229, https://doi.org/10.1002/term.2653.
[58] S. Schreivogel, et al., Load-induced osteogenic differentiation of mesenchymal stromal cells is caused by mechano-regulated autocrine signaling, J Tissue Eng Regen Med 13 (2019) 1992–2008, https://doi.org/10.1002/term.2948.
[59] Z.Y. Zhang, et al., A comparison of bioreactors for culture of fetal mesenchymal stem cells for bone tissue engineering, Biomaterials 31 (2010) 8684–8695, https://doi.org/10.1016/j.biomaterials.2010.07.097.
[60] D. Yang, et al., The immune reaction and degradation fate of scaffold in cartilage/bone tissue engineering, Mater Sci Eng C Mater Biol Appl 104 (2019) 109927, https://doi.org/10.1016/j.msec.2019.109927.
[61] L. Chung, et al., Key players in the immune response to biomaterial scaffolds for regenerative medicine, Adv. Drug Deliv. Rev. 114 (2017) 184–192, https://doi.org/10.1016/j.addr.2017.07.006.
[62] M. Chen, et al., Substrate stiffness modulates bone marrow-derived macrophage polarization through NF-kappaB signaling pathway, Bioact Mater 5 (2020) 880–890, https://doi.org/10.1016/j.bioactmat.2020.05.004.
[63] B. Taciak, et al., Evaluation of phenotypic and functional stability of RAW 264.7 cell line through serial passages, PloS One 13 (2018), e0198943, https://doi.org/10.1371/journal.pone.0198943.
[64] J.W. Hartley, et al., Expression of infectious murine leukemia viruses by RAW264.7 cells, a potential complication for studies with a widely used mouse macrophage cell line, Retrovirology 5 (2008) 1.
[65] G. Hulsart-Billstrom, et al., A surprisingly poor correlation between in vitro and in vivo testing of biomaterials for bone regeneration: results of a multicentre analysis, Eur. Cell. Mater. 31 (2016) 312–322, https://doi.org/10.22203/ecm.v031a20.
[66] L. Luo, et al., The effects of dynamic compression on the development of cartilage grafts engineered using bone marrow and infrapatellar fat pad derived stem cells, Biomed. Mater. 10 (2015), 055011, https://doi.org/10.1088/1748-6041/10/5/055011.